

Pressure Hallucinations and Patterns in the Brain¹

Eric Tkaczyk
Purdue University

Abstract: Whirling domains of geometric patterns seen after pressure on the eyeball, known as phosphenes, have been observed for over 2000 years, but their source of origin remains a mystery. The study tested the feasibility of phosphene generation in the cortex through the action of decreased retinal input. This decrease is elicited by the retinal ischemia that accompanies prolonged pressure. A simple Wilson-Cowan network model of interactions between excitatory and inhibitory neurons receiving tonic thalamic inputs was used. Assuming that inhibitory neurons normally receive disproportionately more retinal input, it was predicted and demonstrated by phase plane analysis of a reduced two-neuron-pair model that decreased retinal input would cause the uniform steady state of the cortex to become unstable via a pitchfork bifurcation, resulting in elementary cortical pattern formation. In a circular, one-dimensional network of 102 neurons, simple stripe patterns were produced by the proposed mechanism. Under the complex logarithmic visuo-cortical mapping, similar two-dimensional patterns could account for commonly observed binocular pressure phosphenes.

1 Introduction

Description of Phosphenes

Other than taking hallucinogenic drugs, there are many ways to induce the perception of intriguing regular, whirling geometric patterns in the visual field. Such patterns can easily be observed by applying continued pressure to both eyeballs. In this case, they are called pressure phosphenes. Phosphenes in general can also be elicited by any of the following methods: staring at a flickering field (Remole, 1974) or a uniform bright field (Tyler, 1978); electrical stimulation of the eyeball (Carpenter, 1973); migraine headaches (Grüsser, 1995); direct electrical (Shakhnovich *et al.*, 1982) or magnetic (Marg and Rudiak, 1994) stimulation of the cortex; extreme convergence of the eyeballs by staring at the nose with crossed eyes (Tyler, 1978); and blows to the head (Walker, 1981). In

¹A similar paper by the same author entitled “A Model for Cortical Pressure Phosphene Generation Based on Disinhibition” appeared in the Winter 2001 issue of the Harvard Journal of Undergraduate Sciences.

what is known as “prisoner’s cinema,” these images can also appear to a person sitting in total darkness for a prolonged period of time (Walker, 1981). For the casual reader, an excellent cursory phenomenological description of pressure and other phosphenes is Jearl Walker’s Scientific American article (Walker, 1981).

Pressure phosphenes were first reported before 400 BC and have subsequently been contemplated by such greats as Plato, Ptolemaeus, Kepler, Boyle, Newton, Descartes, and others (Grüsser and Hagner, 1990). Observations of pressure phosphenes lead to the idea that an integral part of the visual process is the production of physical light by the eyeball, and this notion persisted into the 18th century (Grüsser *et al.*, 1989). More recently, other than a mere curiosity, phosphenes have been of interest in engineering a visual prosthesis (Everitt and Rushton, 1978; Record *et al.*, 1989).

The past few decades have witnessed the rise of an extensive literature devoted to phosphenes, but the most authoritative paper describing pressure phosphenes is still Christopher Tyler’s analysis (Tyler, 1978). Tyler proposes five different classes of phosphenes according to probable site of origin: (1) retinal neural network; (2) retinal blood vessels; (3) choroidal blood vessels; (4) monocular visual pathway; and (5) binocular pressure phosphenes. For our model, we are interested in binocular pressure phosphenes because of the greater likelihood, as Tyler surmises, of a purely cortical origin. In addition to their limitation to binocular pressure, the cortical origin of these patterns is supported by their similarity to flicker phosphenes, which are also presumed to be of cortical origin (Tyler, 1978).

Tyler describes binocular pressure phosphenes as follows:

One type of binocular pattern, which is rarely seen with monocular deep pressure, is an apparently regular pattern of cells of a grid, similar to a chessboard or triangular-element sunflower pattern. The patterns are very repetitive and periodic, as though they were made up from gratings and chessboard forms rather than the blobs and blotches which are produced by electrical stimulation of the eye. This regularity also contrasts with the pattern of retinal and choroidal blood vessels seen on releasing the deep pressure, which branch in all directions in a much more random fashion.

It is particularly evident that these patterns are graded in fineness from the fovea to the periphery, as though they were proportional to the size of retinal or cortical receptive fields as a function of eccentricity.

Tyler’s depictions of this sunflower pattern are reproduced in Figure 1.

The Wilson-Cowan Model

The Wilson-Cowan equations, whose general form is given in the Methods section of this article, have been accepted as one of the predominant ways to realistically model active networks of neurons, as they are based on fundamental interactions of firing neurons. Based on the primary responses one firing neuron

can invoke in another neuron onto which it synapses, the equations divide neurons in a given network into two types: excitatory and inhibitory. The Wilson-Cowan equations, with proper parameter sets, easily depict the phenomenon of lateral inhibition in the cortex, whereby firing neurons tend to excite neurons in their vicinity but inhibit neurons farther away (*pers. corr.*, Ermentrout).

Ermentrout (1999) has shown, through Wilson-Cowan models of visual cortex neurons, that upsetting the delicate balance between excitation and inhibition in the visual cortex leads to pattern formation and spectacular visual effects. Once the normal balance is upset, the phenomenon of lateral inhibition begins to take over, and groups of neurons start to fire together, suppressing the surrounding neurons. When this occurs over the regularly structured visual cortex, simple geometric patterns of firing neurons emerge.

Disinhibition

One of the ways by which the balance of excitation and inhibition in a neural network can be upset is the phenomenon of disinhibition. Many neural networks, in their normal state, have a notable extent of internal or external sources of inhibitory neural input. Disinhibition is the result of any action that carries such a normally inhibited neural network to a state with a far lesser degree of inhibition.

Mathematical Visuo-Cortical Transformation

An important consideration for modelling cortical generation of visual phenomena is the nature of the mapping of the visual field in the cortex. Ermentrout and Cowan have worked extensively in this area in modelling hallucinations (Murray, 1989). Here, the retinal image is described in polar coordinates (r, θ) and the transcribed cortical image is described in Cartesian coordinates (x, y) (Murray, 1989):

$$\begin{aligned} x &= \alpha \ln \left[\beta r + (1 + \beta^2 r^2)^{1/2} \right] \\ y &= \alpha \beta r \theta (1 + \beta^2 r^2)^{-1/2}, \end{aligned}$$

where α and β are physiologically determined parameters.

Close to the fovea ($r \ll 1$), this is approximated by:

$$\begin{aligned} x &\sim \alpha \beta r \\ y &\sim \alpha \beta r \theta \end{aligned}$$

More than a solid angle of about one degree from the fovea, a sufficient approximation is:

$$\begin{aligned} x &\sim \alpha \ln [2\beta r] \\ y &\sim \alpha \theta \end{aligned}$$

Thus, over most of the visual field, the transformation can be represented accurately as a complex logarithmic mapping, where the point on the retina, denoted

by the complex coordinate z , is mapped to the cortical point with complex coordinate w :

$$\begin{aligned} w &= x + iy = \alpha \ln[2\beta r] + i\alpha\theta = \alpha \ln[z] \\ z &= 2\beta r e^{i\theta} \end{aligned}$$

One of the most obvious results of this specific mapping is the retinal magnification factor, whereby patterns closer to the center of the visual field take up more space in the cortex than those further out (Murray, 1989). Thus, a regular pattern in the visual cortex could explain Tyler's observation that binocular pressure phosphenes are graded in size from the fovea to the periphery. Furthermore, the nature of the complex logarithmic mapping means that simple geometric patterns like bars and square tessellations of activity in the cortex would correspond to very exciting patterns in the visual field (Fig. 2), not dissimilar to Tyler's original pressure phosphene patterns (Fig. 1). Thus, the current study is concerned simply with generating such simple patterns in the cortex, which might account for phosphenes appearing in the visual field.

2 Methods

Proposed Mechanism

The immediate result of applying direct force is an increase in pressure in the fluid of the eyeballs. The increased intra-ocular pressure gradually reduces retinal perfusion values to near zero and results in ischemia (Tyler, 1978). This causes a diminution of spontaneous activity transmitted through the optic nerve to the lateral geniculate nucleus and eventually to the excitatory and inhibitory neurons of the visual cortex. If inhibitory neurons in the visual cortex normally receive disproportionately more input, then the reduced overall input will disrupt the existing cortical balance in favor of excitation. When the uniform state then becomes unstable, spatial patterns spontaneously emerge. Thus, the proposed mechanism for phosphene generation is pattern formation in the visual cortex when disinhibition occurs in the neural network as a result of decreased retinal input.

As another possibility, Grüsser *et al.* (1989) considered the direct deformation of the retina by stretching and compression. However, our ischemic model is further supported by the appearance of phosphenes after cerebral lesions affecting the visual pathway (Vaphiades *et al.*, 1996; Kasten *et al.*, 1998; Kishi *et al.*, 1998).

The Wilson-Cowan Model

As the Wilson-Cowan model proved to be a successful testing paradigm in studies of hallucinations (Ermentrout, 1999), this is the model of choice to test the proposed mechanism for phosphene generation. A parameter, λ , is incorporated into the general Wilson-Cowan equations to represent the decreased retinal input that is the proposed catalyst of phosphene generation. Thus, the

Wilson-Cowan equations as the accepted model for neural networks is modified to incorporate the proposed mechanism and test the plausibility of phosphenes being the result of patterns arising directly in the visual cortex as the result of decreased retinal input.

The general model for phosphene generation in the visual cortex consists of a layer of excitatory and inhibitory neurons whose naturally decaying firing rates (E for excitatory, I for inhibitory) over distance (x) and time (t) are described by the differential equations:

$$\begin{aligned}\frac{d}{dt}E(x, t) &= -E(x, t) + fe(Jee(x) \cdot E - Jie(x) \cdot I - te + lre) \\ \tau \frac{d}{dt}I(x, t) &= -I(x, t) + fi(Jei(x) \cdot E - Jii(x) \cdot I - ti + lri),\end{aligned}$$

where the evolution of the firing rates are dictated by three types of synaptic inputs:

1. $Jee(x) \cdot E$ and $Jei(x) \cdot E$ are convolutions for the synaptic inputs from all excitatory neurons onto an excitatory or inhibitory neuron, respectively.
2. $Jie(x) \cdot I$ and $Jii(x)$ are inhibitory inputs, convolved over surrounding inhibitory neurons.
3. re and ri are the normal spontaneous retinal inputs to the excitatory and inhibitory neurons, respectively. These are weighted by the proportion λ , which can be reduced to represent reduction in total retinal input to the visual cortex. These are the parameters that differentiate this model from the general Wilson-Cowan equations.

te and ti are the input thresholds to induce firing of the excitatory and inhibitory neurons, respectively. t is the time constant of the inhibitory neurons' response, normalized to exclude any time constant for excitatory neurons from the equations. The synaptic response functions (fe and fi) are standard logistic functions.

Setting ri to be greater than re and then decreasing λ tests the feasibility of the proposed mechanism for disinhibition. Ermentrout (1998) has successfully used similar models in studying LSD trails and hallucinations. The previous work, however, studied different mechanisms to elicit the disinhibition causing these phenomena, such as changing firing thresholds to simulate the presence of drugs. The novelty of this particular study is the attempt to create the disinhibition causing pattern formation merely as the result of decreased external inputs to the neural network.

Immediate implementation of the Wilson-Cowan equations of the general model for phosphene generation described above in a full network of many excitatory and inhibitory neurons provides less insight than progressing through simplified situations to build to a final network realization of the model. Thus, analysis of the model was conducted in three parts. First, the model was examined in the case of only one inhibitory and one excitatory neuron. Next,

the model was implemented in one pair of inhibitory and one pair excitatory neurons. Finally, after sufficient insight was gained, the model was applied to a ring network of 51 pairs of excitatory and inhibitory neurons.

Phase Plane Analysis

Since the objective was to determine variations in stability under decreased retinal input in the adapted Wilson-Cowan model, the mathematical tool of phase plane analysis proved to be extremely useful. To a great extent, the stabilities of different states of the simplified implementations of the model under varying parametric conditions were analyzed in a two-dimensional phase space with Bard Ermentrout's XPPAuto package². Phase plane analysis is covered in detail in books by Strogatz (1996), Blanchard *et al.* (1998), and Edelstein-Keshet (1988), but a brief overview of the fundamental concepts is provided below.

The phase space is the set of all possible conditions of the variables in any differential equation model. Since the model is deterministic, the way the variables evolve from each point in the phase space is uniquely determined. When only two independent variables are present, the two-dimensional phase space is called the phase plane, and analysis is particularly simple and useful. When the adapted Wilson-Cowan model above is simplified to one excitatory and one inhibitory neuron, their firing rates are the two independent variables. The phase plane can then be represented as a set of two axes, each corresponding to the firing rate of a different neuron of the model. Thus, each point in the phase plane is a potential set of initial conditions, since it is a unique combination of firing rates of the two neurons. From these initial conditions, firing rates of the neurons change according to the deterministic model, until reaching a steady state, tracing out curves known as trajectories. Because each trajectory is determined uniquely by the initial conditions and the governing equations, no two trajectories can continue after intersection between them. Otherwise, another trajectory with initial conditions at the intersection would not have a unique path to follow. An example of a phase plane is shown in Figure 3, showing a sample trajectory as a dark solid line. The other elements appearing in the figure will be described presently.

The governing system of differential equations can be set to zero and solved to reveal the fixed points (also called steady states), which are the points where neither of the variables changes in value. Thus, any trajectory with initial conditions exactly on the fixed point will not travel anywhere. This amount of precision in initial conditions is of course only mathematically possible, so it is important to classify fixed points as stable if all trajectories passing through the vicinity of the fixed point are drawn into it, and unstable if arbitrarily small perturbations away from the fixed point cause trajectories to leave it. By linearizing the governing equations around the fixed point, eigenvalues can be calculated whose signs and magnitudes determine the stability of the fixed points. If the real parts of all eigenvalues are negative, the fixed point is stable. If they are

²available at <http://www.pitt.edu/~phase>

positive, it is unstable, and if one is negative and the other is positive, the fixed point is a saddle point possessing a special kind of instability. All trajectories passing through the general vicinity of the saddle-point are swept away along the direction of the eigenvector corresponding to the positive eigenvalue, except for that infinitesimal subset of trajectories that lead exactly to the eigenvector corresponding to the negative eigenvalue. Figure 3, which continues to be described presently, shows two fixed points: one stable fixed point, and one saddle point.

When the time derivative of one of the variables is set to zero, the corresponding solution curve in the phase space is called a nullcline. Nullclines are the set of points in the phase space where one of the variables does not change with time. Thus, each variable in the model has a corresponding nullcline, and fixed points occur at any intersection of all the nullclines. In a phase plane, trajectories crossing the nullcline for the variable of the ordinate or the abscissa are horizontal or vertical, respectively, at the intersection. Nullclines section the phase plane into areas with different signs of the change in variables, and thus the orientation of trajectory segments along a nullcline are opposite on different sides of a fixed point. Thus, with little calculation, it is a simple matter to determine the qualitative flow throughout a two dimensional phase plane by examining the nullclines. Some sample arrows indicating the horizontal and vertical trajectory direction along the nullclines are marked in Figure 3.

The manner in which the nullclines intersect is especially informative with respect to the stability of the fixed points. Due to the specific form of the Wilson-Cowan equations in the phosphene generation model, whenever the nullcline of the variable plotted on the abscissa has a greater slope at intersection than the nullcline of the ordinate, the fixed point is a saddle point. In the opposite case, the fixed point is stable. The more tangentially the nullclines cross, the more likely it is that a further parameter change will change the stability or even existence of a fixed point. Studying eigenvalues and eigenvectors and using some index theory, these observations can be proven in a non-complicated manner. It is even easier, however, to accept these results intuitively from the general flows in the phase plane determined along the nullclines or to use XPPAuto, which automatically linearizes the system of equations around the fixed points to numerically evaluate stabilities. Some more sample phase planes, nullclines, fixed points, and trajectories are shown in Figure 4. Their importance will be described in the Results section.

Although a saddle point is unstable, its negative eigenvalue manifests itself in the form of a stable manifold. This curve is an exceptional set of initial conditions along which all trajectories go to the saddle point, rather than being repelled away. Because the stable manifolds are actually trajectories themselves, they form an uncrossable barrier for other trajectories, which partitions the phase plane into basins of attraction, each of which can have only one steady state, which attracts all trajectories beginning in the basin (Fig. 5).

3 Results

Single Pair of Neurons

Initially, the model was implemented with one excitatory neuron coupled to an inhibitory neuron:

$$\begin{aligned} E' &= -E + f(aee \cdot E - aie \cdot I - te + \lambda re) \\ I' &= \frac{-I + f(aei \cdot E - aii \cdot I - ti + \lambda ri)}{\tau} \\ f(u) &= \frac{1}{1 + e^{-u}}, \end{aligned}$$

where the equations correspond to the general Wilson-Cowan model described above. I.e., aee is the weight of the synaptic input of the excitatory neuron onto itself, corresponding to $Jee(x)$ in the general model, and similarly, aie , aei , and aii , correspond to $Jie(x)$, $Jei(x)$, and $Jii(x)$, respectively.

The desired goal of decreased stability under decreased λ was produced with the following set of parameters: $aee = 10$, $aie = 6$, $te = 2.7$, $re = 0.72$, $ti = 3.42$, $ri = 2.05$, $\tau = 1$, $aei = 6$, $aii = 1.45$. It was observed that increasing re shifted the E nullcline up, whereas increasing ri shifted the I nullcline to the left. Decreased λ , as expected, had the opposite of these effects, and because of the original relation of the nullclines (Fig. 4A), a less stable tangential intersection resulted at the new fixed point with decreased retinal input (Fig. 4B).

The selection of these parameters was not based on actual physiological measurements. Rather, they were obtained simply through variation within a reasonable range to demonstrate that a simplified neural network obeying these classical neuron firing rate models could exhibit decreased stability under decreased input.

Two Coupled Pairs of Neurons

Next, the model was tested in a simple network consisting of two coupled pairs of an excitatory and an inhibitory neuron:

$$\begin{aligned} E1' &= -E1 + f(aee \cdot E1 - \frac{aie(I1 + c \cdot I2)}{1 + c} - te + \lambda re) \\ E2' &= -E2 + f(aee \cdot E2 - \frac{aie(c \cdot I1 + I2)}{1 + c} - te + \lambda re) \\ I1 &= f(aei \cdot E1 - ti + \lambda ri) \\ I2 &= f(aei \cdot E2 - ti + \lambda ri) \\ f(u) &= \frac{1}{1 + e^{-shp \cdot u}}, \end{aligned}$$

where $E1$ and $E2$ are the firing rates of each of the two excitatory neurons, and $I1$ and $I2$ are those of the inhibitory neurons. The constant c regulates the extent of lateral inhibition, and the standard reduction assumption of fast inhibition ($\tau \rightarrow 0$) has been taken so the model can be analyzed in a two-dimensional

phase plane (Gutkin, 1999). The lateral inhibition has been normalized to make the parameter aie meaningful.

Under the parameter set $aie = 6$, $ri = 0.6$, $shp = 1.5$, $c = 1$, $te = 0.5$, $ti = 1.5$, $ae = 7.5$, $re = 0.3$, $aei = 5$, the desired change in stability of the uniform steady state is observed. In the normal state with full retinal input ($\lambda = 1$), there are three stable fixed points and two saddle points in the $E1$ - $E2$ phase plane (Fig. 5). Two of the stable points represent a high firing rate of only one neuron, but all initial conditions with nearly equal firing rates of the two excitatory neurons fall into the basin of attraction of the uniform steady state. Thus, minor perturbations and irregularities would not result in pattern formation. However, a bifurcation occurs when λ is decreased past 0.8937. The stable uniform steady state suddenly transforms into a saddle point whose stable manifold is none other than the line of exact equality between $E1$ and $E2$. The two new stable fixed points, which appear on either side of the new saddle point, are slightly disparate in the firing rates of the two neurons (Fig. 6 A). When λ is decreased further, the new stable states coalesce with the original saddle points, annihilating each other at $\lambda = 0.7169$ and leaving behind only the unstable uniform fixed point and the ever-present, extremely disparate stable nodes (Fig. 6 B, C). Thus, trajectories starting arbitrarily close to uniform firing rates jump to the divergent states, which is the beginning of pattern formation.

The changing steady states around the uniform fixed point are summarized in the bifurcation diagram of Figure 7. The bifurcation diagram, read from right to left, shows the $E1$ coordinate of the fixed points as they evolve over decreasing λ . The bifurcation where the stable uniform state suddenly becomes unstable around $\lambda = 0.8937$ is clearly visible, as is the disappearance of any other stable states as λ decreases past 0.7169.

51 Pairs of Neurons

After insight had been gained from looking at the simplified versions of the model, the general model for phosphene generation was implemented in an array of neurons. Using the same squashing synaptic response function as for the coupled pairs of neurons ($f(u) = (1 + e - shp \cdot u)^{-1}$), the equations were applied to a circularly connected, one-dimensional network of 51 excitatory and 51 inhibitory neurons. Additional random inputs in the range $[0, 0.01]$ were given to excitatory neurons to seed the pattern formation. λ was set as an exponentially decreasing function of time ($\lambda = \lambda_0 e^{-\lambda_1 t}$) to observe the evolution of spatial pattern formation. For the convolutions, each neuron took equal normalized input from a varying number of neighboring inhibitory neurons, and from a different number of neighboring excitatory neurons. The radius of neighboring neurons from which excitatory or inhibitory input was taken is the representation in the phosphene generation model of the varying widths of excitatory and inhibitory synapses from a given neuron. The radii were kept in the four to ten neuron range, since typically in a neural network of the brain, any given neuron will be directly and strongly influenced by a nontrivial number of neighbors, but not a major proportion of the neurons in the tissue.

Under the parameter set $Jee = 7.5$, $Jej = 5$, $Jie = 5$, $Jij = 0$, $te = 0.5$,

$ti = 1.5$, $re = 0.3$, $ri = 0.4$, $\lambda_0 = 1$, $\lambda_1 = 0.02$, $t = 0.2$, $shp = 1.5$, convolution over a radius of seven excitatory neurons and four inhibitory neurons produced in one dimension the desired stripe-like patterns thought to be indicative of observed pressure phosphenes (Fig. 8). As soon as the radius of excitatory neuron input was extended close to the radius of inhibitory neuron input, no such patterns were obtained (Fig. 9). An interesting phenomenon that might merit further study is the appearance of spatio-temporal oscillations when inhibition is slowed to levels near excitation (Fig. 10).

Once again, the parameters applied to all three implementations of the adapted Wilson-Cowan Model introduced in the Methods section were not based upon any experimental physiological data, but were selected to conceptually and mathematically test the plausibility of the proposed mechanism.

4 Discussion

The examination of the different simplifications of the Wilson-Cowan phosphene generation model supports the plausibility of disinhibition in the visual cortex resulting from decreased retinal input as the cause of pressure phosphenes. Already in the reduced two-neuron-pair model, the decrease in stability of the uniform steady state and resulting jump to disparate firing rates of neurons strongly supports the proposed mechanism for phosphene generation. The emergence of patterns in the full, one-dimensional network is even more promising. A shortcoming of the model, however, is that these patterns do not emerge with broader excitatory than inhibitory connections. In the physical visual cortex, the inhibitory interneurons normally are connected only locally while the excitatory pyramidal cells typically branch much further (Kandel and Schwartz, 1985), and for the model to accurately represent this would require broader inhibitory than excitatory radii of influencing neurons.

However, the current study is by no means exhaustive. In the current study, when convolution was taken over a radius of neurons, it was assumed that all the neurons in this radius had equally strong inputs onto the neuron whose firing rate was being calculated. Perhaps more typical ‘‘Mexican hat’’ lateral inhibitions resulting from using Gaussian-shaped convolutions (Ermentrout, 1998) would help overcome this obstacle.

The model also does not explain Tyler’s observation of the different sizes of gratings and blank TV screens which interrupt the regular pattern. In the spirit of Tyler’s hypothesis that these result from interactions between different layers of visual cortex (Tyler, 1978), it is implausible that a complete understanding of phosphenes could be obtained without taking very detailed anatomical data into account. The first step would be using scanning electron microscope images to determine typical connection distances for interneurons and pyramidal cells in a layer of the visual cortex. Next, the model would have to be implemented over a two dimensional array. The input weighting parameters would have to be varied until spatial frequencies of clinically observed phosphene patterns would correspond to the spatial frequency in the scaled down two dimensional array

of neurons. Finally, a third dimension could be added to the model to depict interactions between different layers of visual cortex.

Nonetheless, even after mere one-dimensional implementation, the proposed simple model does explain the essential attributes of deep pressure phosphenes which so mystified Tyler when he wrote:

“the monocular point array and the binocular geometric patterns must be regarded as indicators of some further selective process in the physiological pathway, a kind of functional Golgi stain by which certain neural activities are elevated into consciousness while the majority of possible discharges remain ignored” (Tyler, 1978).

Following the example of Ermentrout’s hallucination work (Ermentrout, 1998), when the domination of lateral inhibition in the disinhibited visual cortex and the retino-cortical magnification factor are taken to be Tyler’s “further selective process in the physiological pathway,” an almost instantaneous explanation arises for the regularity of typical pressure phosphene patterns with increasing size from the fovea to the periphery. Examination of the Wilson-Cowan equations implemented in the pressure phosphene generation model in this study lead to the conclusion that reduced retinal input onto the visual cortex can easily lead to a pattern-forming disinhibited state that could account for the phenomenon of pressure phosphenes.

5 Acknowledgements

The author would like to thank the Center for the Neural Basis of Cognition Summer Undergraduate Training Program for sponsorship and Bard Ermentrout for his outstanding mentorship.

6 Figures

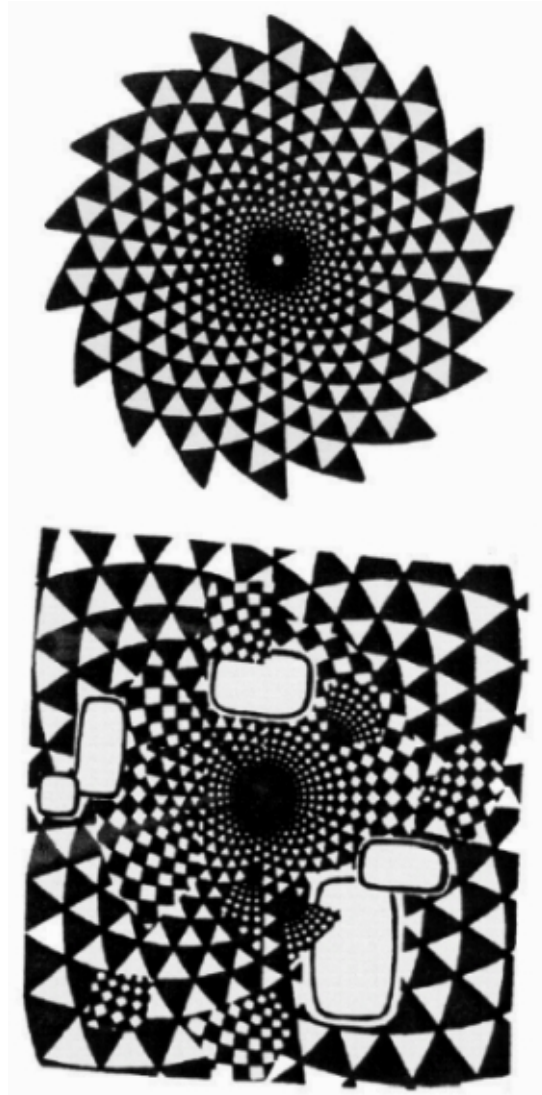


Figure 1: Typical observed binocular pressure phosphenes from Tyler's paper (1978).

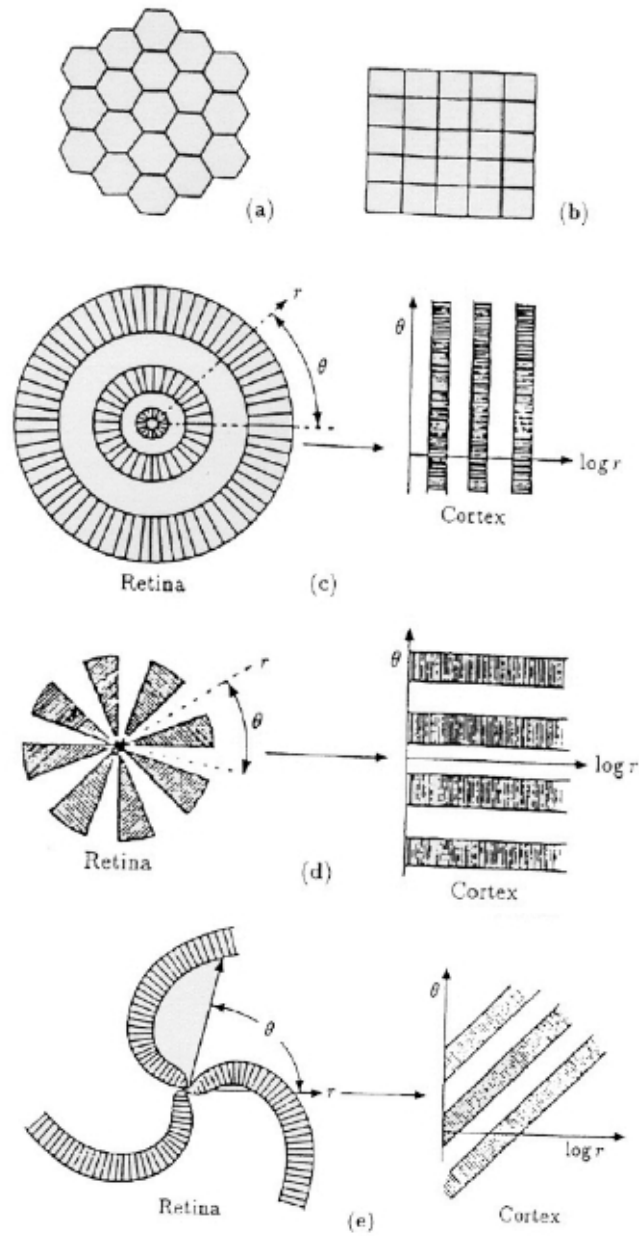


Figure 2: The visuo-cortical mapping. On the left are the images seen in the visual field and on the right are the corresponding patterns produced in the cortex (from Murray, 1989).

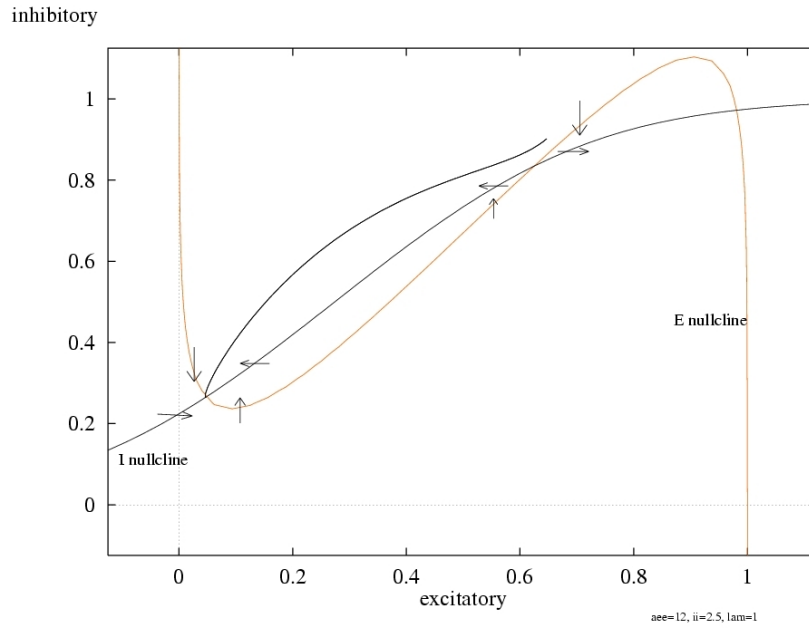


Figure 3: Phase plane and nullclines of firing rates in the simple two-neuron Wilson-Cowan model with increased recurrent excitation ($aee = 12$) and increased inhibitory input ($ri = 2.5, \lambda = 1$). The meaning of the specific parameters producing this phase plane is described in Part IV under “Single Pair of Neurons.” Arrows show directions of flow determined along the nullclines. The solid line is a sample trajectory starting near a saddle point being attracted to a stable fixed point. As the model has not been correlated yet to physiological measurements, all units in the model, and thereby neuron firing rates, appear unitless.

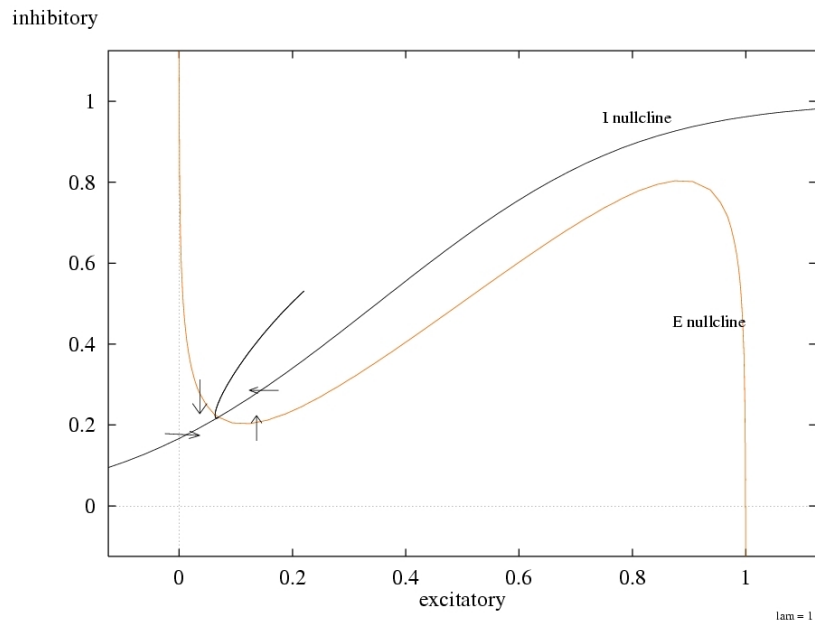


Figure 4 A: Phase plane of the two-neuron model. Full retinal input ($\lambda = 1$). Because the E nullcline drops below the I nullcline, we know from the nullcline-dictated flow that the fixed point at their intersection is stable.

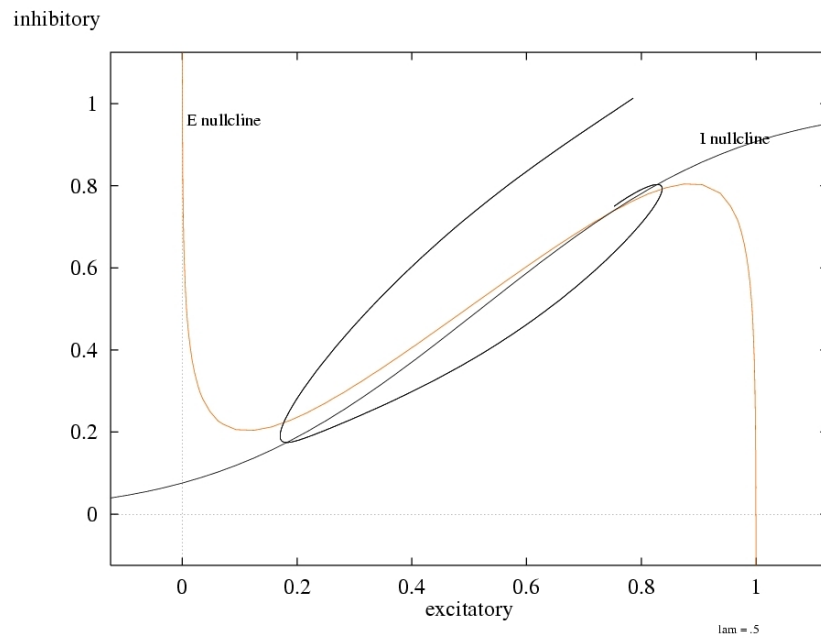


Figure 4 B: Phase plane of the two-neuron model. Decreased input ($\lambda = 0.5$). The nullclines now intersect more tangentially and the lesser degree of stability resulting from less negative eigenvalues is evidenced by the greater winding of the sample trajectory before it is finally pulled into the stable fixed point.

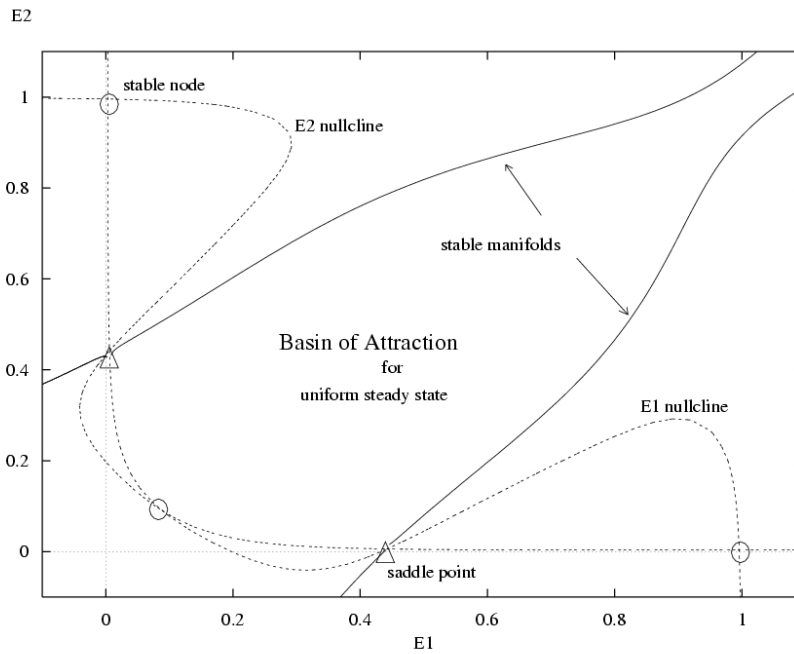


Figure 5: Phase plane of the firing rates of the two different excitatory neurons ($E1$ and $E2$) in the simplified two-neuronal pair model. With full retinal input ($\lambda = 1$), there are five fixed points. The stable manifolds of the two saddle points (triangles) split the phase plane into three basins of attraction — one for each stable node (circles). Note the delicacy at the stable node with equal firing rates of both neurons, which is implied by the nearly tangential intersection of nullclines. However, the basin of attraction for this uniform state is large.

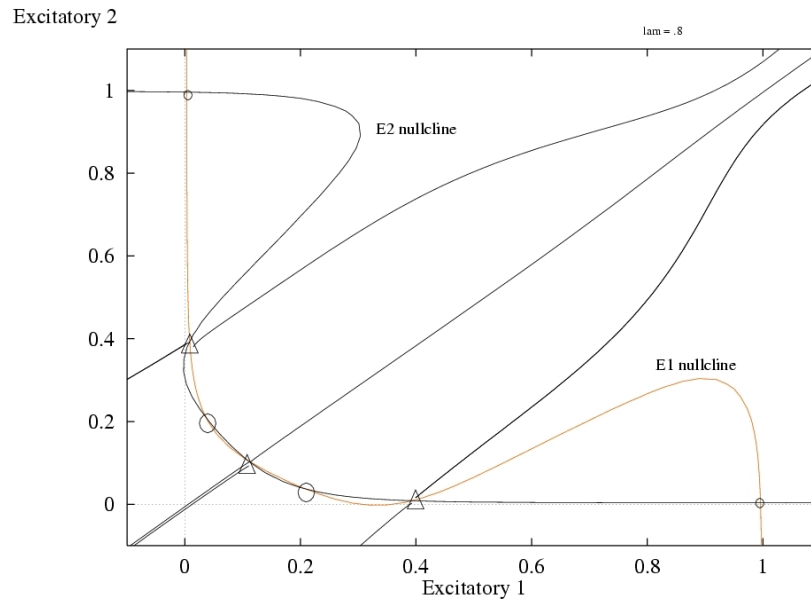


Figure 6 A: When retinal input is slightly decreased (here $\lambda = 0.8$), the large basin of attraction for the uniform steady state splits in half as two new stable states appear and the uniform fixed point transforms into a saddle point whose stable manifold is the line $E2 = E1$.

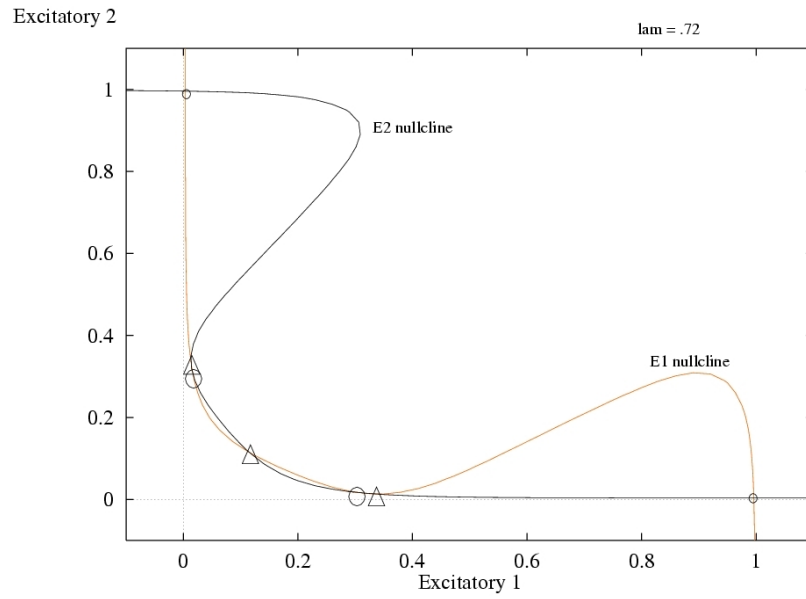


Figure 6 B: Further decrease in λ (here $\lambda = 0.72$) causes the coalescence and mutual annihilation of these new steady states with two saddle points.

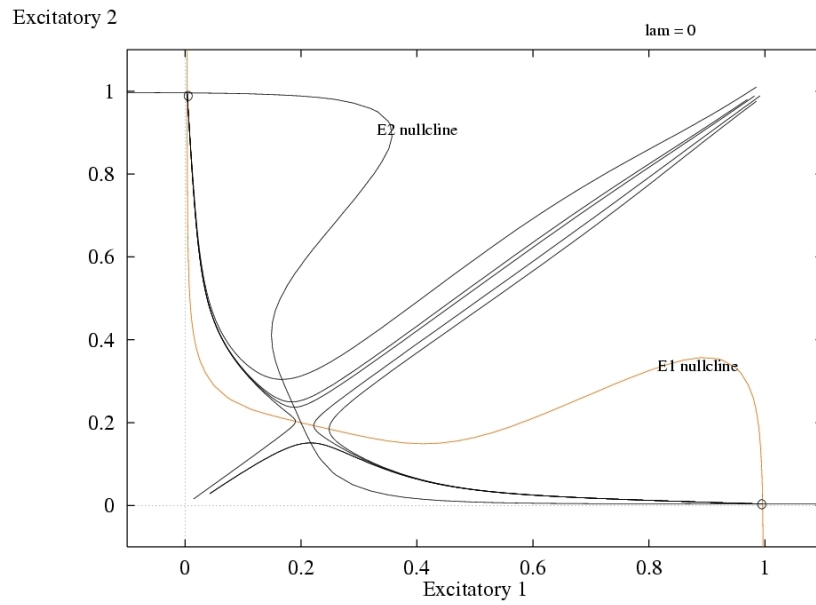


Figure 6 C: Finally, with no retinal input ($\lambda = 0$), the nullclines have pulled apart, and only an unstable uniform fixed point and two divergent stable nodes remain. *See text for explanation.*

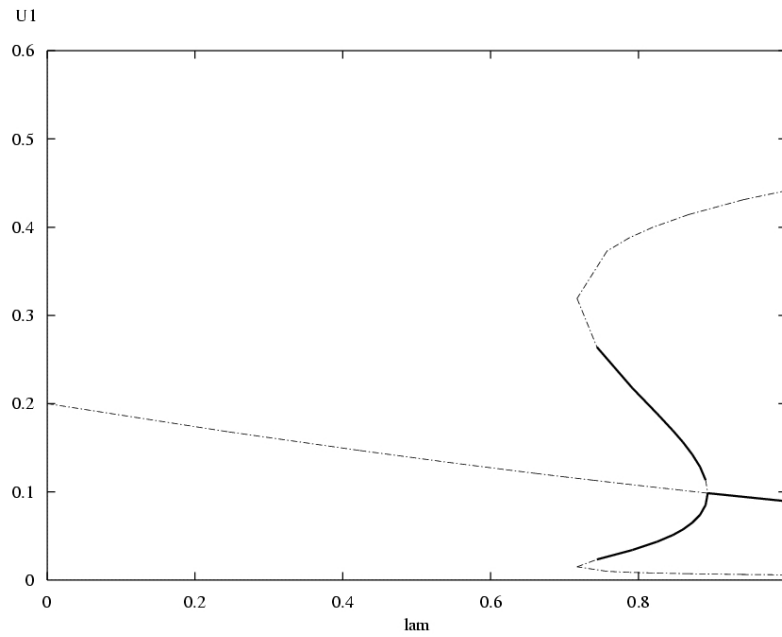


Figure 7: Bifurcation diagram showing the appearance, disappearance, and change in stability over varying λ of steady states close to the uniform state. Solid lines represent stable nodes; dotted lines represent saddle points. The two extreme stable nodes, where one neuron is firing maximally and the other not at all, are not shown here.

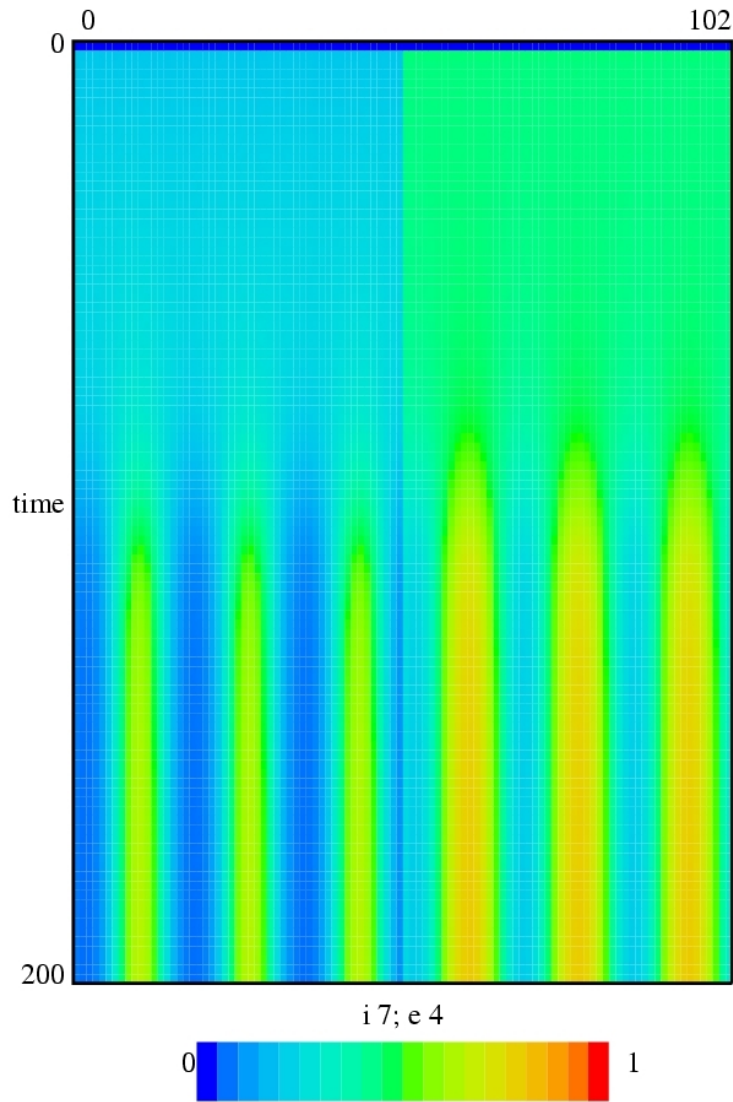


Figure 8: An array plot of firing rates, coded by brightness, when the full model is run with excitatory convolutions of a four neuron radius and inhibitory convolutions over a seven neuron radius. The first 51 columns each show the firing rate of a different excitatory neuron, the last 51 show the inhibitory neurons. The bar at the bottom shows how the brightness corresponds to the firing rates, ranging from 0 to 1 in the usual unitless quantity used in the phase planes. Retinal input decays with time, which is on a linear scale down the ordinate. Thus, looking down the picture from top to bottom gives a sense of how the pattern in the band evolves as retinal input decreases.

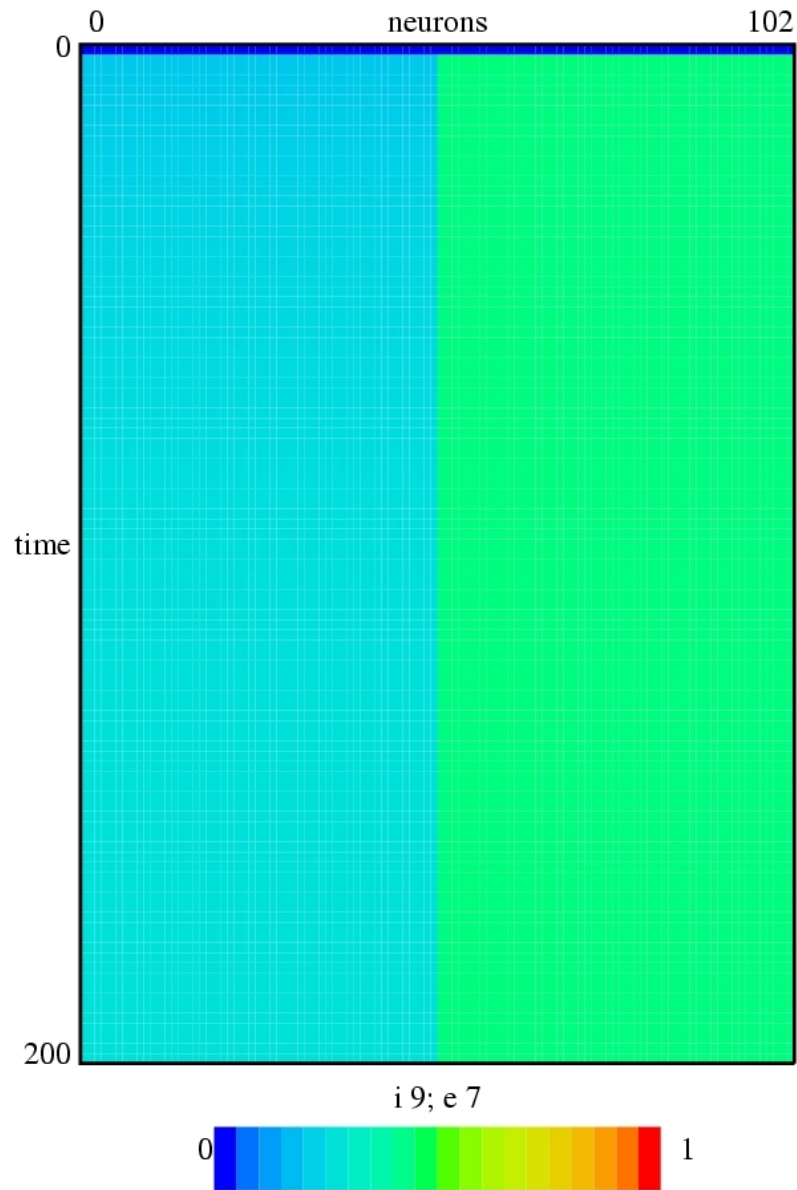


Figure 9: When the same simulation is run with inhibition extending over a nine neuron radius and excitation extending over seven neurons, no pattern emerges.

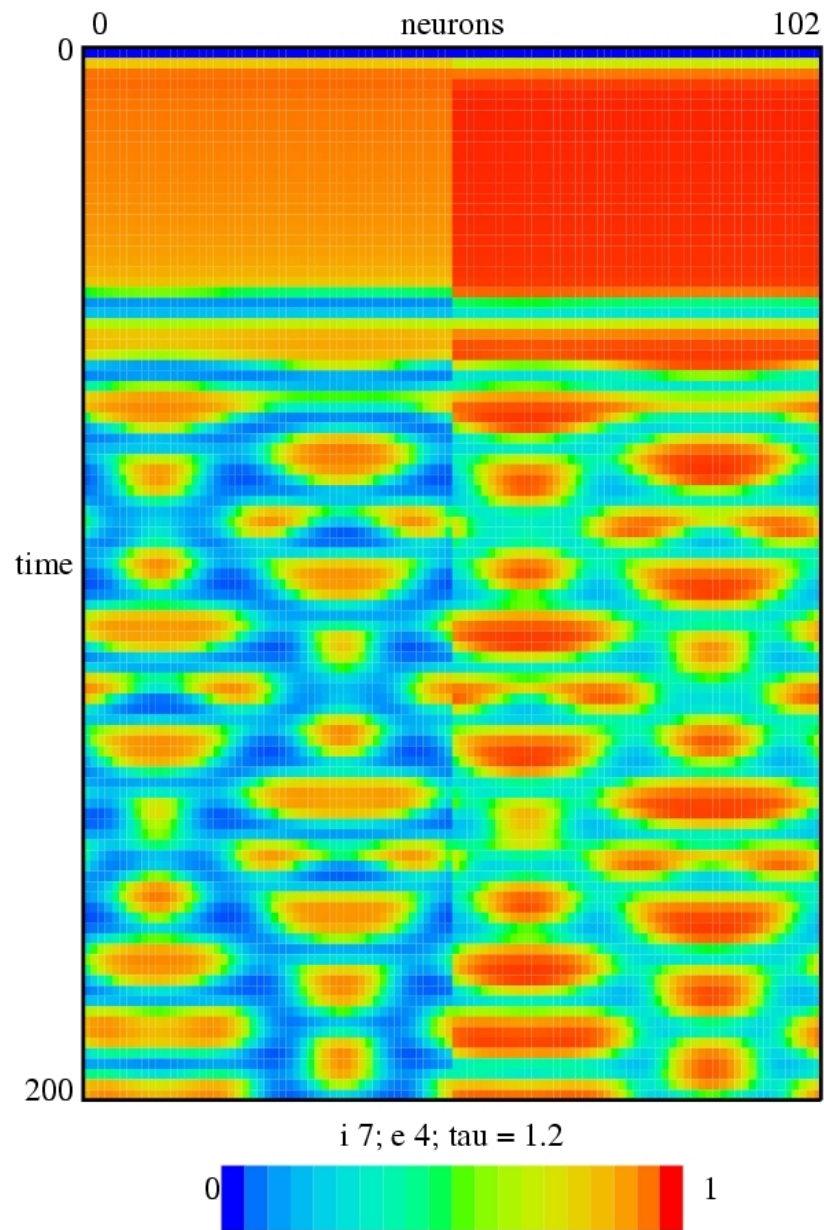


Figure 10: Appearance of oscillations with the same parameter set as in Figure 8, except an increased time constant for the inhibitory neurons from 0.1 to 1.2.

References

- [1] Blanchard, P, Devaney, RL, Hall, GR. (1998) *Differential Equations*. Pacific Grove, CA: Brooks/Cole Pub. Co.
- [2] Carpenter, RHS (1973) Contour-like phosphenes from electrical stimulation of the human eye: some new observations. *J. Physiol.* **229**, 767–785.
- [3] Edelstein-Keshet, L (1998) *Mathematical Models in Biology*. New York: Random House.
- [4] Ermentrout, GB (1998) Neural networks as spatio-temporal pattern-forming systems. *Rep. Prog. Phys.* **61**, 353–430.³
- [5] Ermentrout, GB (1999) The excited cortex LSD trails, phosphenes, and other visual confections. *Eighth Annual Computational Neuroscience Meeting* presentation. Abstracts p. 201.
- [6] Everitt BS, Rushton DN (1978) A method for plotting the optimum positions of an array of cortical electrical phosphenes. *Biometrics* **34**, 399–410.
- [7] Grüsser O.-J. (1995) Migraine phosphenes and the retino-cortical magnification factor. *Vision Res.* **35**, 1125–34.
- [8] Grüsser O.-J., Grüsser -Cornhels U, Kusel R, Przybyszewski AW (1989) Responses of retinal ganglion cells to eyeball deformation: a neurophysiological basis for “pressure phosphenes.” *Vision Research* **29**, 181–194
- [9] Grüsser O.-J., Hagner M (1990) On the history of deformation phophenes and the idea of internal light generated in the eye for the purpose of vision. *Doc. Ophthalmol.* **74**, 57–85.
- [10] Gutkin B, Ermentrout GB, Chow C, Rinzel J, Izhikevich E, Abbott L (1999) Mathematical reduction of complex neural models: methods and uses of reduced models. *Eighth Annual Computational Neuroscience Meeting* workshop. Abstracts p. 7.
- [11] Kandel E R, Schwartz J H (1985) *Principles of Neural Science*. New York: Elsevier.
- [12] Kasten E, Muller-Oehring E, Poggel D, Sabel BA (1998) Chronic visual hallucinations and illusions following brain lesions. A single case study. *Fortschr. Neurol. Psychiatr.* **66**, 49–58.
- [13] Kishi T, Ishino H, Naganuma R (1998) Insight into phosphene: a case with occipital lobe damage. *Gen. Hosp. Psychiatry* **20**, 260–261.
- [14] Marg E, Rudiak D (1994) Phosphenes induced by magnetic stimulation over the occipital brain: description and probable site of stimulation. *Optom. Vis. Sci.* **71**, 301–311.

³available at <ftp://euler.math.pitt.edu/pub/bardware/classes/nnetsrev.ps>

- [15] Murray, JD (1989) *Mathematical Biology*. New York: Springer-Verlag.
- [16] Record P, Williams E, Hitchcock E, Ahmon M (1989) Computer-controlled stimulation in the assessment of electrical characteristics for cortical phosphene generation for a visual prosthesis. *J. Med. Eng. Technol.* **13**, 52–56.
- [17] Remole, Arnulf (1974) Luminance thresholds for perceived movement in a flickering field. *J. Opt. Soc. Am.* **64**, 1133.
- [18] Shakhnovich AR, Ogleznev Kya, Abakumova Lya, Tishchenko LS, Razumovskii AE (1982) Phosphene formation during electrical stimulation of the visual cortex. *Hum. Physiol.* **8**, 34–39.
- [19] Strogatz, Steven H. (1996) *Nonlinear Dynamics and Chaos*.
- [20] Tyler, Christopher W (1978) Some new entoptic phenomena. *Vision Research* **18**, 1633–1639.
- [21] Vaphiades MS, Celesia GG, Brigell MG (1996) Positive spontaneous visual phenomena limited to the hemianopic field in lesions of central visual pathways. *Neurology* **47**, 408–417.
- [22] Walker, Jearl (1981) About phophenes: luminous patterns that appear when the eyes are closed. *Scientific American* **244**, 174.